Check for updates

3D printed gelatin/hydroxyapatite scaffolds for stem cell chondrogenic differentiation and articular cartilage repair†

Jianghong Huang,‡[a,b] Zhiwang Huang,‡[a] Yujie Liang,‡[b,c] Weihao Yuan,[d] Liming Bian, [ID][d] Li Duan,[a,e] Zhibin Rong,[f] Jianyi Xiong,*[a] Daping Wang*[a,e,g] and Jiang Xia [ID] *[b]

Acute injury of the articular cartilage can lead to chronic disabling conditions because of the limited self-repair capability of the cartilage. Implantation of stem cells at the injury site is a viable treatment, but requires a scaffold with a precisely controlled geometry and porosity in the 3D space, high biocompatibility, and the capability of promoting chondrogenic differentiation of the implanted stem cells. Here we report the development of gelatin/hydroxyapatite (HAP) hybrid materials by microextrusion 3D bioprinting and enzymatic cross-linking as the scaffold for human umbilical cord blood-derived mesenchymal stem cells (hUCB-MSCs). The scaffold supports the adhesion, growth, and proliferation of hUCB-MSCs and induces their chondrogenic differentiation *in vitro*. Doping HAP in the gelatin scaffold increases the fluidity of the hydrogel, improves the gelation kinetics and the rheological properties, and allows better control over 3D printing. Implanting the hUCB-MSC-laden scaffold at the injury site of the articular cartilage effectively repairs the cartilage defects in a pig model. Altogether, this work demonstrates the 3D printing of gelatin-based scaffold materials for hUCB-MSCs to repair cartilage defects as a potential treatment of articular cartilage injury.

[a]*Department of Orthopedics, Shenzhen Intelligent Orthopaedics and Biomedical Innovation Platform, Guangdong Artificial Intelligence Biomedical Innovation Platform, Shenzhen Second People's Hospital, the First Affiliated Hospital of Shenzhen University Health Science Center, Shenzhen, 518035, China. E-mail: jianyixiong@126.com, wangdp@mail.sustech.edu.cn*

[b]*Department of Chemistry, and Center for Cell & Developmental Biology, School of Life Sciences, the Chinese University of Hong Kong, Shatin, Hong Kong SAR, China. E-mail: jiangxia@cuhk.edu.hk*

[c]*Shenzhen Kangning Hospital, Shenzhen Mental Health Center, Shenzhen, Guangdong, 518020, China*

[d]*Department of Biomedical Engineering, the Chinese University of Hong Kong, Shatin, Hong Kong SAR, China*

[e]*Guangzhou Medical University, Guangzhou, Guangdong, 511436, China*

[f]*Shijiazhuang Maternity and Child Health Hospital, Shijiazhuang, Hebei, 050093, China*

[g]*Department of Biomedical Engineering, Southern University of Science and Technology, Shenzhen, 518055, China*

†Electronic supplementary information (ESI) available: The score chart of International Cartilage Repair Society (ICRS) macroscopic evaluation of cartilage repair. The score chart of the ICRS visual histological assessment scale. The primers used for RT-qPCR analysis. The rheological properties of the gelatin/HAP scaffolds with different compositions of HAP. The physical properties of the scaffolds: swelling and moisture content. The IR spectra of the gelatin scaffold, gelatin/HAP scaffold and HAP alone. Western blot analysis of the protein expression level on different scaffolds. Histological analysis of the cell culture on different scaffolds *in vitro*. Surgical procedures of the cartilage damage and scaffold/MSC transplantation. Immunohistochemical staining of collagen II, collagen X and MMP-13. See DOI: 10.1039/d0bm02103b

‡ These authors contributed equally to this work.

Significance statement

Cartilage injuries affect the elderly and the young worldwide. However, no effective drugs or therapies are currently available. Implantation of mesenchymal stem cells (MSCs) provides a viable therapeutic option, but suitable tissue scaffolds are required to support the proliferation of the cells and direct their differentiation. Here we show that HAP doping into the gelatin scaffold regulates the rheology of the hydrogel and the gelation time for 3D printing. Implanting the gelatin/HAP scaffold and hUCB-MSCs effectively repairs knee cartilage defects in a pig model, providing a superior biomaterial for the treatment of cartilage damage.

Introduction

A range of conditions such as trauma, genetic factors, obesity, inflammation, *etc*. can cause articular cartilage damage, defects, or degeneration, which may further develop into disabling diseases.[1,2] Since articular cartilage does not have blood supply, nerve tissues, or lymphatic vessels, its self-repair ability is very limited. Therefore, once injury occurs, cartilage can quickly deteriorate. With the aging of the population,

heightening obesity rate and increasing incidence of sport injuries, joint damage or cartilage injuries will become the fourth disabling disease worldwide.[3–5] Methods to repair articular cartilage defects include microfracture, autologous osteochondral transplantation, osteochondral allograft transplantation, autologous chondrocyte implantation, transplantation bioengineered chondrocyte sheets, and cell-free multilayered nano-composite scaffolds.[6–12] Each method, however, has its own limitations, and the clinical needs have not been met.

Implantation of stem cells at the damaged cartilage sites, together with guided differentiation of the stem cells *in situ*, provides a viable method for the repair of cartilage damage. Biomaterials with articulately designed 3D frameworks are indispensable as scaffolds for stem cells to adhere, proliferate, and differentiate. 3D bioprinting is an emerging powerful technology to devise such scaffolds. One of the commonly used 3D printing techniques is microextrusion, in which the bioink is extruded through a nozzle onto a substrate from a pressurized syringe barrel. The bioinks for microextrusion need to have balanced rheological properties, including viscosity, yield stress and shear thinning behavior.[13–15] Higher viscosity leads to high extrusion pressure through the nozzles and increases the shear force during the extrusion.[16–18] Polymeric biomaterials used as bioink include natural biopolymers such as polysaccharides (hyaluronic acid, alginate, and agarose)[19,20] and proteins (collagen, fibrin, and silk).[21–23]

Among these biomaterials, gelatin, the hydrolysate of collagen, provides interactions with stem cells through the collagen binding proteins, and thereby promotes cell proliferation, adhesion, and migration.[24–27] Due to its excellent biocompatibility, low immunogenicity, and appropriate biodegradability, gelatin has been developed as hemostatic wound dressings, vascular stents, drug carriers, tissue engineering implanted stents, and others.[28–31] However, as a protein hydrolysate, gelatin-based constructs lack the mechanical strength for use as tissue engineering scaffolds. Here we use two methods to modulate the properties of the gelatin hydrogel scaffolds to fit the requirement of 3D bioprinting and supporting stem cells in cartilage damage sites *in vivo*. First, enzymatic cross-linking can stabilize the fluidic material to maintain its 3D frame. Transglutaminase (EC 2.3.2.13) crosslinks the side chains of the amino acids of the proteins, and is therefore used as biological glue for proteins.[32–35] Doping heterologous materials such as the mineral hydroxyapatite (HAP) may also increase the strength of hydrogel bioink. The biogenic apatite HAP has several physicochemical properties that make it an attractive candidate for diagnosis and treatment of disease and augmentation of biological tissues.[36] Moreover, hybrid HAP-containing biomaterials provide a promotive scaffold for chondrocytes. For example, Jia and co-workers showed that collagen/HAP scaffolds are amenable to cell adhesion, homogeneous cell distribution, and maintenance of the morphology of natural chondrocytes.[37] Jiang and co-workers also showed that a collagen/HAP film better supports the growth and preserves the phenotype of chondrocytes compared with collagen alone.[38] Jamal and co-workers proved that HAP-based colloidal gels facilitate the proliferation and migration of chondrocytes.[39] HAP containing hybrid materials were also reported to promote the chondrogenesis of stem cells. For example, Spadaccio and co-workers developed poly-L-lactic acid/HAP electrospun nanocomposites which induced chondrogenic differentiation of human MSCs.[40] In a recent report, Calabrese engineered collagen/HAP hybrid materials and showed the promotion of the chondrogenic differentiation of stem cells.[41] In this report, we develop 3D-printed HAP-doped, enzyme crosslinked gelatin scaffolds, demonstrate the capability of the scaffolds to support the proliferation and chondrogenic differentiation of hUCB-MSCs, and show the promotion of cartilage repair by the cell-laden gelatin/HAP scaffold in pigs (Scheme 1). Altogether, our report features an effective method of modulating gelatin hydrogels for 3D printing (HAP-doping and enzyme crosslinking) and gelatin/HAP scaffolds that can promote chondrogenic differentiation of hUCB-MSCs both
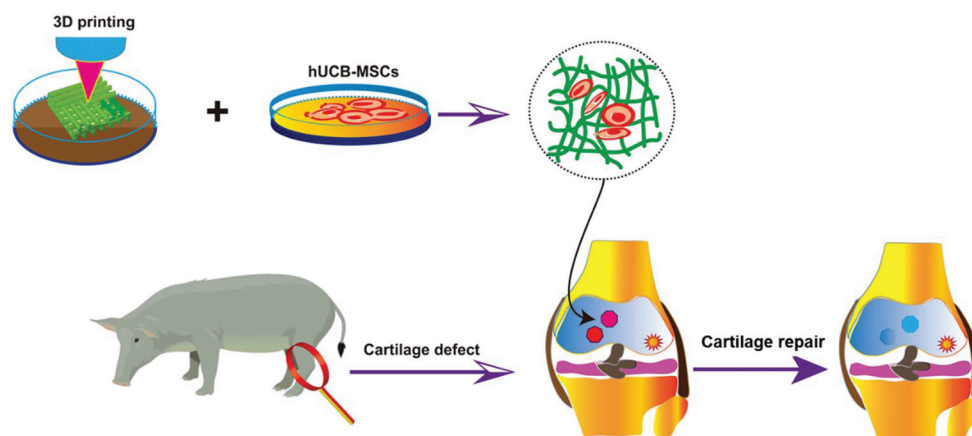
Scheme 1 Schematic illustration of 3D-printed gelatin scaffolds, co-cultured with hUCB-MSCs for chondrogenic differentiation and repair of cartilage defects in the joints.

in vitro and *in vivo* in a pig model of cartilage repair, which has not been reposrted in the literature to our knowledge. Pigs are used as model animals to evaluate the therapeutic efficacy because of the high similarity of the pig cartilage to the human cartilage in the anatomical structure, thickness, physiological function and biomechanics.

Results

3D printing of transglutaminase cross-linked gelatin hydrogel scaffolds

Gelatin scaffolds were printed based on the thermo-responsive properties of gelatin, doping of HAP, and enzymatic cross-linking. Briefly, gelatin dissolved in deionized water (10%, w/v) was added with different percentages of HAP to produce hydrogel materials, and the rheological properties of the hybrid materials were analysed (ESI Appendix, Fig. S1†). 10% of gelatin with 5% volume weight of HAP gave the best gelation kinetics and rheological properties that best fit the requirement of 3D printing, and this composition was then employed to produce bioink to print gelatin scaffolds. Two types of scaffolds were produced: 10% of gelatin alone or 10% of gelatin with 5% volume weight of HAP. The scaffolds were then immersed in 1% (w/v) of *Streptoverticillium mobaraense* transglutaminase for enzymatic crosslinking for 6 h. This then gave a colorless gelatin scaffold and an opal gelatin/HAP scaffold (Fig. 1A and B). After freeze-drying, the scaffolds maintained the skeletons with uniform pores (Fig. 1C and D). Under a scanning electron microscope (SEM), the pores were found to be 10–50 μm (Fig. 1E–H). The two materials showed similar porosity rates, 85.26 ± 2.09% for the gelatin scaffold and 81.29 ± 2.05% for the gelatin/HAP scaffold (Fig. 1I). The porous structure provides a large surface area for cell attachment and promotes the proliferation and migration, exchange of nutrients, and chondrogenic differentiation of MSCs.[42–44] Both materials swell in buffer, reaching equilibrium within 4 h (ESI Appendix, Fig. S2†). The gelatin scaffold contains a higher amount of moisture than the gelatin/HAP scaffold, 91.47 ± 0.42% *vs.* 84.29 ± 0.75%. IR spectra showed characteristic protein vibration peaks, including amide A bands at 3290 cm^{-1} and 3300 cm^{-1}, indicating the presence of hydrogen bonds. Amide I bands were found at around 1638 cm^{-1} and 1633 cm^{-1} corresponding to the stretching vibration of the C=O bond, suggesting that the secondary structures of the peptides were retained. Amide II bands were found at 1550 cm^{-1} and 1541 cm^{-1}, indicating the presence of the C–N stretching vibration or N–H bending vibrations. Amide III bands appeared at 1239 cm^{-1} and 1238 cm^{-1}, indicating that the scaffolds maintained the triple helix structure of gelatin. The signals at 1450 cm^{-1} also indicate the presence of gelatin molecules. The presence of HAP is evidenced by the peaks at 550 cm^{-1}, 560 cm^{-1}, 605 cm^{-1}, 965 cm^{-1}, 1025 cm^{-1} and 1030 cm^{-1}. The IR spectrum of the gelatin/HAP scaffold shows a superposition of those of gelatin and HAP, indicating that these two materials are bound together through physical interactions instead of chemical crosslinking (ESI Appendix, Fig. S3†).

Rheological analysis of the scaffolds

The changes in the elastic modulus G' (storage modulus) and the viscous modulus G'' (loss modulus) of the hydrogels were continually monitored during the gelation (Fig. 2A). Pure gelatin hydrogels showed a rapid gelation process. The initial elastic modulus G' and the viscous modulus G'' are very small when the gelatin is in the fluid state. After 100 s, the elastic modulus G' and the viscous modulus G'' increased dramatically and showed a cross point at 147 s, which indicates the sol–gel transition of gelatin. With the extension of time, both the elastic modulus G' and viscous modulus G'' gradually plateaued, with G' being higher than G''. At this point, the crosslinking of the hydrogels is saturated. HAP doping allows slowing down the gelation kinetics. The elastic modulus G' and the viscous modulus G'' remained at the initial values for a longer time and increased much slower than the gelatin hydrogel, indicating that the gelation efficiency of the gelatin/HAP system is relatively low. 3D printing of the gelatin hydrogel may clog the printing needle, especially during high-resolution printing. By slowing down the gelation kinetics, HAP doping allows more freedom in the design of the 3D struc-
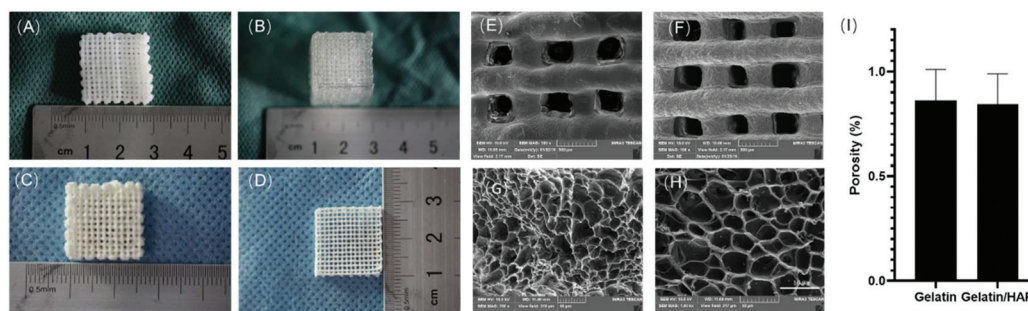

Fig. 1 Characterization of the 3D-printed scaffolds. The gelatin/HAP scaffold (A) and gelatin scaffold (B) before lyophilization. The gelatin/HAP scaffold (C) and gelatin scaffold (D) after lyophilization. SEM images of the gelatin/HAP scaffold (E) and gelatin scaffold (F) at 100× magnification. Enlarged SEM images (1000×) of the gelatin/HAP scaffold (G) and gelatin scaffold (H), and the porosity of the gelatin/HAP scaffold and gelatin scaffold (I).
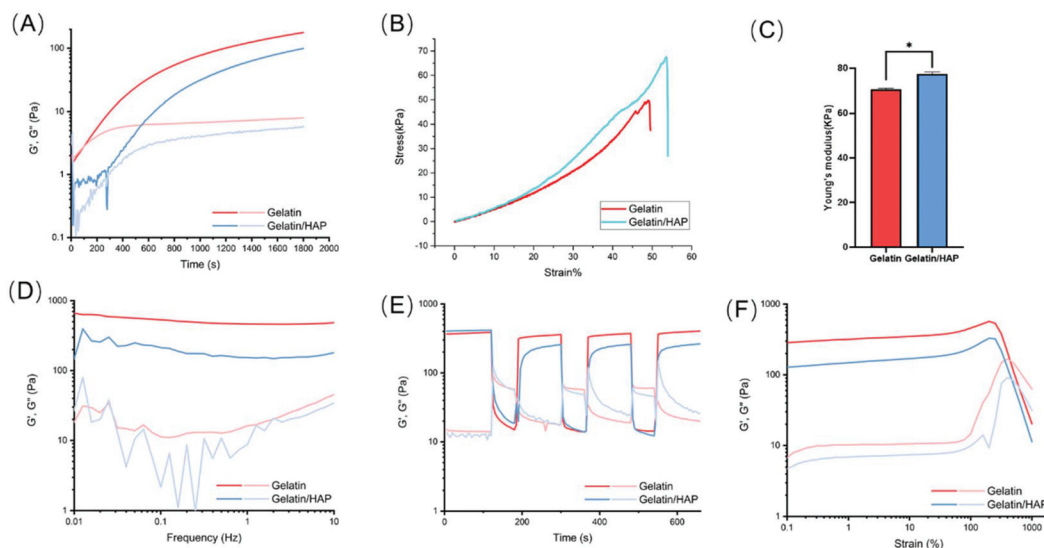
Fig. 2 Rheological properties of the gelatin and gelatin/HAP scaffolds. (A) The time sweeps. (B) Stress−strain curves. (C) Elastic modulus. (D) Frequency sweeps. (E) Shear thinning. (F) Strain sweeps of gelatin and gelatin/HAP hydrogel.

tures, and reduces the clogging of the needles during the printing and shaping process of the scaffolds.

The addition of HAP can also enhance the mechanical strength of the scaffold, as shown by the increased compression modulus, from 70.49 ± 0.67 kPa (gelatin scaffold) to 77.35 ± 0.96 kPa (gelatin/HAP scaffold) (Fig. 2B and C). Based on the frequency sweep, both the hydrogels showed a frequency-independent behavior, but still possessed viscoelastic properties according to the ratio of loss modulus and storage modulus. In the shear-thinning and strain sweep tests, both materials showed good anti-shearing properties and only exhibited a gel–sol transition over a shear strain of 500%. Moreover, the hydrogels show a reversible gel–sol–gel transition under alternatively applied shear strains of 1% and 600%, which corresponds to their self-healing property and injectability (Fig. 2D–F).

Proliferation and differentiation of hUCB-MSC cells on scaffolds

We next explored whether the scaffolds can induce the differentiation of human umbilical cord blood-derived mesenchymal stem cells (hUCB-MSCs) (Fig. 3A). The cytotoxicity of the hydrogel materials was first measured by culturing hUCB-MSCs in the extracted solutions of the scaffolds. Although HAP doping slightly increased the cytotoxicity, the extract solutions supported a high cell viability of >75% (Fig. 3B). Both materials supported the proliferation of hUCB-MSCs indicated by a continuous increase of the cell population (Fig. 3C). The scaffold materials also provide a platform for cell migration. Fluorescently stained hUCB-MSCs primarily adhered to the pores of the scaffolds on day 1, with very few on the edges. Gradually more cells grew and migrated to the interior of the scaffolds (Fig. 3D). Comparatively, the cells grew into a higher density and migrated more evenly in the

gelatin scaffolds than the gelatin/HAP scaffold. Taken together, both the scaffolds are highly biocompatible and can support the adhesion, proliferation, and migration of the MSCs.

Next, we explored whether the scaffolds could direct the differentiation of hUCB-MSCs.[45] RT-PCR indicated that after being cultured on the scaffolds for 7 days, hUCB-MSCs on the gelatin/HAP scaffold showed the upregulation of ACAN and COL2A1, whereas the cells on the gelatin scaffold did not show any difference from the control. On days 14 and 21, a significant increase of the early chondrogenic factor SOX9 and two later factors ACAN and COL2A1 is observed (Fig. 3E). COL1A1 remained unchanged, indicating the formation of hyaline cartilage instead of fibrocartilage. Consistent with this result, western blotting analysis showed that hUCB-MSCs on the gelatin/HAP scaffold expressed a significantly higher level of collagen II, aggrecan, and SOX9, and a markedly lower level of MMP-13 and collagen X at the protein level after 21 days of cell culture (ESI Appendix, Fig. S4†). The gelatin/HAP scaffold is therefore superior to the gelatin scaffold in this regard, suggesting that HAP enhances the chondrogenic differentiation potential of gelatin. Further evidence was provided by histological analysis of the hUCB-MSCs on the scaffolds *in vitro*. Briefly, hUCB-MSCs were seeded on the gelatin scaffold or the gelatin/HAP scaffold, respectively, and the gelatin scaffold only without stem cells is considered as a blank control. After 14 or 21 days, the cell cultures were then sectioned and stained with Toluidine Blue and Alcian Blue (ESI Appendix, Fig. S5†). The higher staining signals on the gelatin/HAP showed that this scaffold promotes the formation of a cartilage-like structure in the cell culture.

Scaffold-supported stem cell therapies of cartilage damage

Next, we explored whether the scaffolds could support stem cell therapy to treat cartilage damage *in vivo*. An animal model
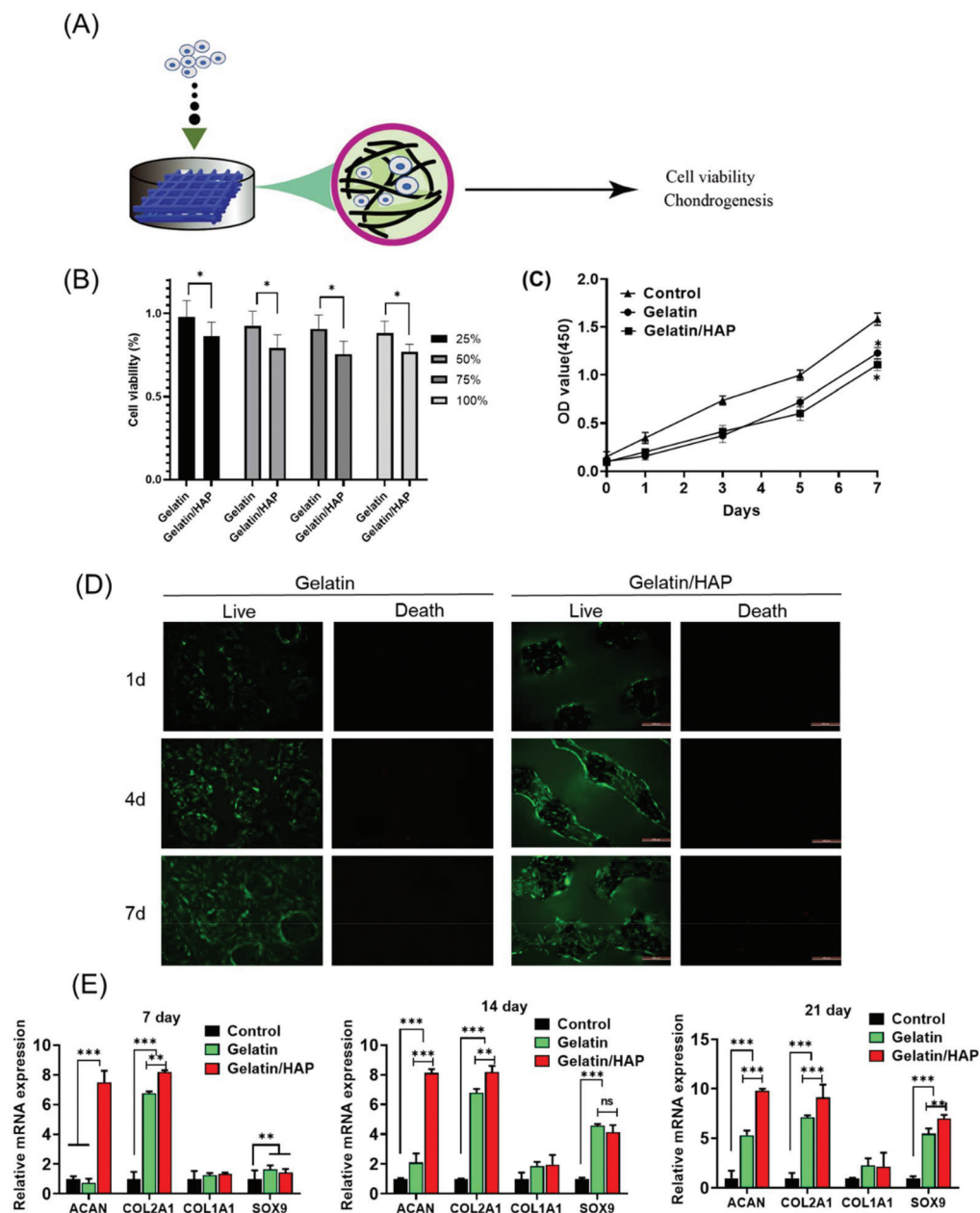
Fig. 3 Proliferation and induction of hUCB-MSCs on scaffolds. (A) Schematic illustration of the experimental design. (B) Cytotoxicity measurement of the scaffold extraction solutions. *, $p < 0.05$. (C) Proliferation of the cells on the scaffolds. (D) Live−death cell staining on the scaffolds. Scale bar, 500 μm. (E) RT-PCR measurement of genes related to chondrogenesis after culture in hydrogels and chondrogenic supplements for 7, 14 and 21 days. $n = 3$. **, $p < 0.01$; ***, $p < 0.001$.

of cartilage injury has been established using Wuzhishan pigs, a miniature pig breed. Pigs are chosen as model animals here because of their large joint area and thick cartilage layer, which resemble those of the human joints. Three square-shaped damage sites were created on the cartilage of the knee joints by surgery. Each site was 10 mm × 10 mm in size and 3 mm in depth (ESI Appendix, Fig. S6†). Three groups of treatments were implemented in each animal. Site I was left as a blank control without implants (Group I). Site II received hUCB-MSCs with the gelatin scaffold (Group II). Site III

received hUCB-MSCs with the gelatin/HAP scaffold (Group III). The animals were sacrificed at week 12 or 24, and the cartilage tissues were dissected and analyzed. These two time points were chosen because clinically patients who received cartilage repair surgeries are often revisited after 3 or 6 months. The overall appearances of the three sites were first evaluated. Apparently, Site III showed a much more complete repair than Sites I and II both after 12 weeks and 24 weeks (a representative picture is shown in Fig. 4A). At 12 weeks, the control group still had a clear visible edge between the damaged site and the
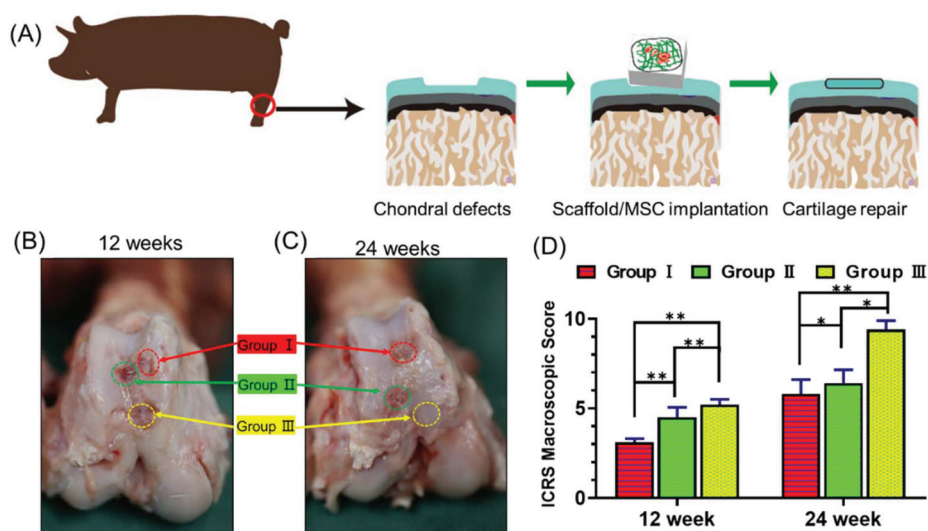
Fig. 4 Scaffold supported MSC cartilage repair in a pig model. (A) Schematic illustration of the experimental procedure. (B and C) Representative images of the damage sites after 12 weeks (B) and 24 weeks (C). (D) ICRS scores of the images. Group I, blank control; Group II, gelatin scaffold + hUCB-MSCs; and Group III, gelatin/HAP scaffold + hUCB-MSCs. Each of the two samples at a time point was evaluated by three researchers independently in a double-blind study. The ICRS scores show the average of six numbers of the two samples for each time point. *, $p < 0.05$; **, $p < 0.01$.

healthy tissue, whereas Site II and Site III showed 50% and 80% repair, respectively. The repair further improved, and the damage repair increased to 70% in Site II and almost complete in Site III at the time point of 24 weeks. The ICRS microscopic scores (ESI Appendix, Table S1†) of the three groups also showed significant differences, with Group III having the
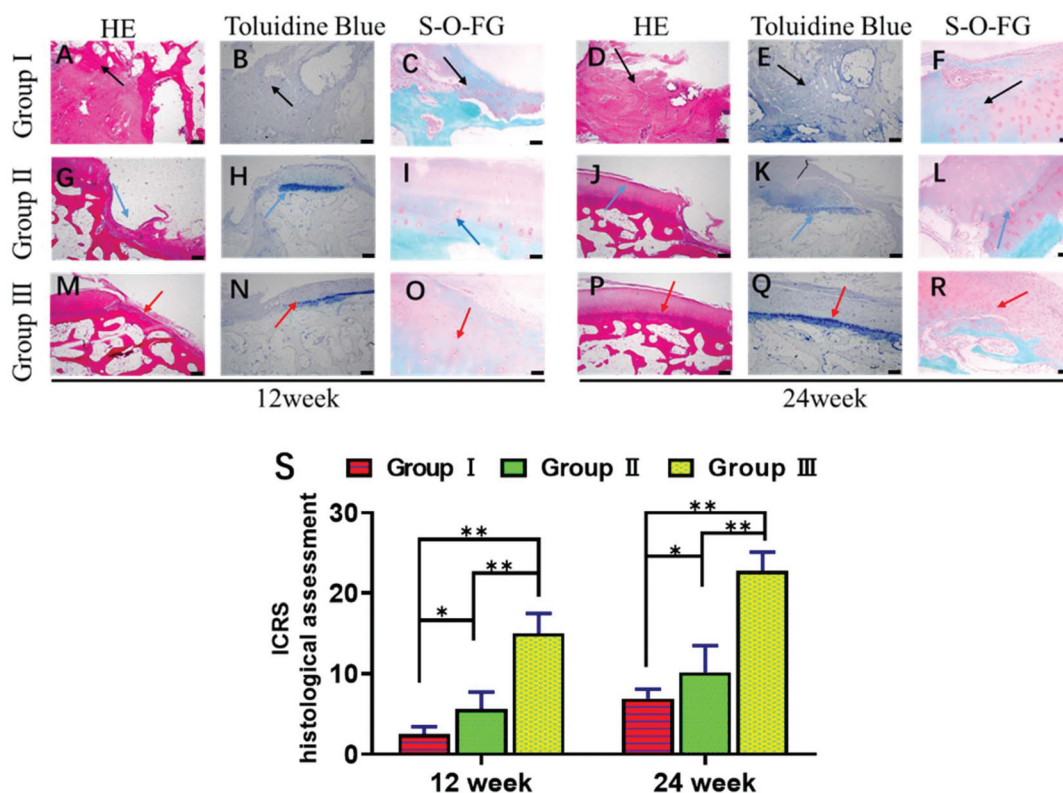

Fig. 5 Images of the cartilage tissues stained by H&E, toluidine blue, and safranin-O−fast green (S-O−FG) (A−R). Black arrows indicate the formation of cavities, fibrous tissues, or inflammatory tissues. Blue arrows indicate the partially repaired cartilage tissues. Red arrows indicate fully repaired cartilage tissues. Scale bar, 100 μm. Each image was evaluated by three researchers independently in a double-blind study. (S) ICRS scores which show the average of the evaluation scores of each image. *, $p < 0.05$; ** p, < 0.01.

highest score among the three groups (Fig. 4B). Group II also showed a significant repair effect but less effective than that of Group III. This experiment shows that both scaffolds can support stem cells to fix cartilage damage, and the gelatin/HAP scaffold gives superior cartilage repair.

This conclusion was further supported by histological analysis of the tissues. In Group I samples, the cartilage damage is visible with the formation of cavities and fibrous tissues after 12 weeks (Fig. 5A–C). The damaged areas reduced after 24 weeks, and were covered by inflammatory tissues (Fig. 5D–F, indicated by black arrows). In comparison, the damaged tissues in Group II showed partial cartilage repair, evidenced by newly regenerated cartilage tissues at the damage sites after 12 weeks (Fig. 5G–I) The regenerated tissues filled up 70% of the cavities after 24 weeks (Fig. 5J–L). The best repair results were seen in Group III samples, in which newly regenerated cartilage tissues almost completely covered the damaged sites after 12 weeks (Fig. 5M–O). After 24 weeks, the cavities were fully covered, and tissues were almost identical as the transparent healthy cartilage (Fig. 5P–R). Numerical evaluations based on the ICRS system (ESI Appendix, Table S2†) quantified the degree of cartilage repair in each group. Both Group II and Group III showed significant repair results with Group III being superior to Group II (Fig. 5S). This result is also consistent with immunohistochemical staining against type II collagen (ESI Appendix, Fig. S7†). We have also tested the hypertrophy markers collagen X and MMP-13 at weeks 14 and 21, which showed a lower level of these two marker proteins in the gelatin/HAP group (ESI Appendix, Fig. S8†). Taken together, the gelatin/HAP scaffold provides a superior support for MSCs for cartilage repair, and HAP doping significantly increases the cartilage repair potential of the gelatin scaffold.

Conclusion and discussion

3D bioprinting is one of the additive manufacturing technologies that can realize the precise assembly of biomaterials and seed cells in the 3D space and the construction of personalized scaffolds. Ideal tissue engineering scaffolds should meet the following conditions:[14–18] excellent biocompatibility, suitable biodegradability to allow substitution by the extracellular matrix and natural tissues, a suitable pore size and porosity to facilitate the exchange of oxygen, nutrients and metabolites, mechanical properties similar to the natural tissues, low toxicity and immunogenicity, strong plasticity, and ease of processing. Here we demonstrate the 3D printing of gelatin scaffolds assisted by enzymatic cross-linking, and HAP doping further strengthens the ability of the gelatin scaffold to promote chondrogenic differentiation of stem cells. HAP doping into the gelatin scaffold slightly decreased the cell viability and proliferation rate *in vitro*, but gained enormous advantage in promoting the chondrogenic differentiation of MSCs and the *in vivo* efficacy of cartilage repair. Using a pig model of cartilage injury, we demonstrated that the combination of the gelatin/HAP scaffold with hUCB-MSCs effectively repaired the damage within 24 weeks. Taken together, the 3D-printed gelatin/HAP scaffold is a new cartilage tissue engineering material for the repair of acute knee cartilage defects. Here we chose a two-step strategy that preforms the scaffold by 3D bioprinting, followed by seeding cells onto the scaffold to allow the attachment before implantation to the diseased sites, instead of using a cell-laden hydrogel as the bioink for printing. In general, this strategy avoids the viability loss due to the shear force during the printing. Specifically, as this gelatin material requires a post-printing enzymatic cross-linking step, the separation of scaffold construction and cell culturing maximizes the cell viability.

3D-printed scaffolds based on synthetic polymer materials have been reported to provide a microenvironment for stem cells and showed promising therapeutic effects in cartilage repair. For example, the work by Dai and co-workers developed factor-releasing polymer scaffolds for cartilage repair.[46–48] Compared with synthetic polymers, gelatin, a protein hydrolysate derived from natural collagen, better mimics the extracellular matrix of the cells in the cartilage, and thereby provides a more friendly environment for implanted cells. Our work also shows a strategy of modulating the fluidity of gelatin by doping with the nanosized form of hydroxyapatite (HAP), a form of the mineral calcium apatite. HAP doping fine-tunes the fluidity and gelation time, optimizes the rheological properties of gelatin hydrogels, and supports the regeneration of damaged joints in a pig model of cartilage injury. HAP-containing biomaterials serve as scaffolds for stem cells and are well explored in the regeneration of bone or cartilage. For example, HAP-based colloidal gels facilitate the adhesion of umbilical cord mesenchymal stem cells.[39] HAP-coated hybrid PLGA/gelatin nanofiber scaffolds enhanced the stem cell differentiation to osteogenic lineage[49] or human MSCs have been shown to take up HAP nanoparticles for osteogenic differentiation.[50] On the other hand, HAP-doped biomaterials also showed chondrogenic activity.[40,41] This then suggests dual differentiation of stem cells on HAP-containing scaffolds through either osteogenic or chondrogenic routes depending on the other components in the scaffold as well as the differentiation media.[51,52] Notwithstanding, the differentiation of stem cells on HAP-containing scaffolds at the sites of cartilage repair in the joints *in vivo* still remains unresolved and awaits further exploration.

Materials and methods

DMEM culture medium, fetal bovine serum, and enzymes were purchased from Thermo Fischer (Massachusetts, US). Gelatin and HAP were products from Sigma (Missouri, US). Transglutaminase was a product from BOMEI (China). CCK-8 agents and live-dead kits were from Dojindo (Maryland, US). Instruments include a fluorescence microscope from Leica (Wetzlar, Germany), a SEM from TESCAN (Brno, Czechia), and a 3D bioprinter CPD1 from SunP Biotech (Beijing, China). Human umbilical cord blood-derived mesenchymal stem cells

(hUCB-MSCs) were purchased from Cyagen Biosciences (Suzhou) Inc. Chondrogenic culture medium: DMEM with high glucose (Invitrogen), 1% ITS (a mixture of recombinant human insulin, human transferrin, and sodium selenite, from Sigma Aldrich), 50 μg ml^{-1} ascorbate-2-phosphate (Sigma Aldrich), 40 μg ml^{-1} L-proline (Sigma Aldrich), and 1 mM sodium pyruvate (Invitrogen). Nano-sized HAP (an average size of around 20 nm according to the manufacturer) in the powder form was purchased from Nanjing Emperor Nano Material Co., Ltd (Jiangsu, China). Wuzhishan pigs were from Wuzhishan pig breeding base of Huada Agriculture, a subsidiary of Shenzhen Huada Gene Co., Ltd.

3D printing of the scaffolds

The 3D model of the scaffolds (20 mm × 20 mm × 10 mm, with an edge distance of 1.5 mm and a layer height of 0.25 mm) was first designed using CAD and transferred to a CPD1 bioprinter. Gelatin powder and HAP were sterilized by Co-60 irradiation. 10% pure gelatin solution and 10% gelatin solution doped with 5% HAP (w/v) were prepared using DI water, respectively. The two solutions were used as bioinks for 3D printing at room temperature before the solutions formed gels. The printed scaffolds were then immersed in 1% transglutaminase solution (w/v) for crosslinking for 6 h.

Porosity and moisture content measurement

Porosity is defined as the volume of the pores over the total volume of the scaffold. Ethanol occupation is used to estimate the volumes here. The 3D scaffolds were lyophilized for 48 h, and the dry weight was measured. The scaffolds were then immersed in absolute ethanol and placed under vacuum until all the pores were fully filled. The weight of ethanol that occupies the pores is calculated as M_p. The weight of ethanol that corresponds to the total volume of the scaffold is calculated as M_T. Porosity is then calculated as M_p/M_T. The samples were measured in triplet. The moisture content was calculated according to the weight loss of the scaffolds after lyophilization. The swelling curves were calculated by measuring the amount of water absorption of the lyophilized scaffolds at different time points.

Rheological analysis

All the rheological tests were performed on a Malvern Lab Plus rheometer. The experiment was conducted using a 20 mm plate rotor, and the gap was set to 0.5 mm. For the time sweep of the gelation process, the pre-solution of the hydrogel was homogeneously distributed between the top and bottom plates of the rheometer. The data were recorded in oscillation mode with a controlled strain of 0.1%, and the frequency was set to 1 Hz. With other parameters unmodified, the frequency sweep was recorded at a strain of 0.1%, and the frequency ramp was from 10 Hz to 0.01 Hz. For the strain sweep, the frequency was kept at 1 Hz, and the strain ramp was from 0.1% to 1000%. For the shear-thinning and self-healing tests, the frequency was set to 1 Hz, and the strain was altered between 0.1% and 600% for three cycles.

Scanning electron microscopy (SEM) analysis

Scaffolds were sliced into samples of 4 mm × 4 mm × 3 mm sizes, fixed in 2.5% glutaraldehyde solution, dehydrated gradually from 50% up to 100% ethanol, displaced with isopropyl acetate, and freeze-dried for 48 h before being processed for SEM imaging.

Proliferation assay

hUCB-MSCs were cultured in DMEM containing 10% FBS and 1% penicillin/streptomycin under 5% CO_2 at 37 °C. The cells were seeded onto the scaffolds at a density of 1.0×10^5 per scaffold. In the control group, the cells were grown on 48 well plates. The numbers of cells were then measured using CCK-8 kits on different days.

Cytotoxicity measurement

Using the full cell culture medium containing 10% FBS as the extraction solution, the scaffolds were immersed and extracted for 72 h at 37 °C at a ratio of 0.1 g scaffold per ml extraction solution. The extraction solution was then diluted and replaced with the original culture, and the cell culture was continued for 24 h before the cell numbers were counted by the CCK-8 assay.

Cell live–dead staining

The cells were seeded on the scaffolds pre-cut into cylinders of 20 mm diameter and 1 mm thickness for 1 d, 4 d and 7 d before staining with calcein-AM (2 μM) and propidium iodide (3 μM) for 30 min at 37 °C before imaging under a fluorescence microscope.

Chondrogenic differentiation assay and RT-PCR

hUCB-MSCs (1×10^5) were seeded on the gelatin scaffold or the gelatin/HAP scaffold in a 6-well plate, and allowed to adhere before adding the medium. The cells seeded without the scaffold were used as the blank control. hUCB-MSCs cultured on the scaffolds in chondrogenic inducing medium for different days were analyzed by RT-qPCR using primers listed in Table S3.† Total RNA from BMSCs was extracted using TRIzol reagent following the manufacturer's instructions (Thermo Fisher). The total RNA preparation (500 ng RNA) was reverse transcribed to cDNA using an RT-PCR system for first-strand cDNA synthesis (Takara, China). Real-time PCR was carried out for 40 cycles of amplification: 95 °C for 15 s and 60 °C for 60 s using SYBR Premix Ex Taq (Takara, China) on a Stratagene Real-Time PCR system (Applied Biosystems, Grand Island, NY, USA).

Animal studies

6-month-old adult Wuzhishan pigs of about 50 kg were used for the experiments. A total of four pigs were used in all the experiments, two pigs for the 12-week experiment and two for the 24-week experiment. Each pig received surgeries in only one knee to minimize the impact on the pig. Pigs were subjected to general anesthesia: intramuscular injection of keta-

mine 6 mg/kg + diazepam 0.2 mg kg^{-1}, and then anesthetized by continuous inhalation administration (ether 0.3 mg kg^{-1}) from the mouth and nose. Damage to the knee cartilage was made by surgeries to create sites of 10 mm × 10 mm size and 3 mm depth. The damage sites are at least 20 mm apart to avoid interference with each other. hUCB-MSC cells were seeded on the scaffolds (1 million cells per slice), allowed to adhere for 4 h, supplemented with growth medium, incubated overnight, and implanted to the damage sites. The animals were sacrificed at 12 and 24 weeks after implantation. Specimens of the knee joints were taken for gross observation, scoring, and tissue sectioning and staining.

Histopathology

Cryo-sectioning of cartilage tissues was done by following a standard procedure. Briefly, the tissue samples were thawed, mounted and refrozen in OCT (optimum cutting temperature compound) embedding media, and then cryo-sectioned into 6 μm thick sections using a Tissue-Tek II cryostat. The sections were either refrozen and stored at low temperatures (−25 °C) or detected immediately. The nuclei were stained with Hoechst 33342. Articular cartilage specimens from Wuzhishan pigs were fixed in 4% paraformaldehyde for at least 72 h and subsequently decalcified in EDTA buffer (20% EDTA, pH 7.4) for 1–2 months. Subsequently, the tissues were embedded in paraffin. The sections (4 μm) were stained with hematoxylin–eosin–saffron, toluidine blue and safranin O–fast green. For immunohistochemistry, the paraffin-embedded sections were processed and stained with rabbit anti-COLII, and then with the DAB Chromogen kit (Servicebio, China).

Study approval. All the animal experiments were approved by the Ethics Committee of Shenzhen University (No. 201906003).

Statistical analysis

SPSS 21.0 was used for data analysis, and the measured data were expressed as mean ± standard deviation ($\bar{\chi} \pm s$). If the data in each group followed the normal distribution and the homogeneity of variance, the single-factor analysis of variance was used for comparison between groups. Otherwise, the Kruskal–Wallis test is used. $p < 0.05$ indicates significant difference.

Conflicts of interest

The authors declare no competing interests.

Acknowledgements

References

1 V. Silverwood, et al., Current evidence on risk factors for knee osteoarthritis in older adults: a systematic review and meta-analysis, Osteoarthr. Cartil., 2015, 23, 507–515.

2 T. R. McAdams, K. Mithoefer, J. M. Scopp and B. R. Mandelbaum, Articular Cartilage Injury in Athletes, Cartilage, 2010, 1, 165–179.

3 N. Maffulli, U. G. Longo, N. Gougoulias, D. Caine and V. Denaro, Sport injuries: a review of outcomes, Br. Med. Bull., 2011, 97, 47–80.

4 E. B. Hunziker, Articular cartilage repair: basic science and clinical progress. A review of the current status and prospects, Osteoarthr. Cartil., 2002, 10, 432–463.

5 S. N. Lambova and U. Muller-Ladner, Osteoarthritis - Current Insights in Pathogenesis, Diagnosis and Treatment, Curr. Rheumatol. Rev., 2018, 14, 91–97.

6 S. Desai, Surgical Treatment of a Tibial Osteochondral Defect With Debridement, Marrow Stimulation, and Micronized Allograft Cartilage Matrix: Report of an All-Arthroscopic Technique, J. Foot Ankle Surg., 2016, 55, 279–282.

7 D. C. Astur, et al., Functional outcomes after patellar autologous osteochondral transplantation, Knee Surg. Sports Traumatol. Arthrosc., 2017, 25, 3084–3091.

8 I. C. Zouzias and W. D. Bugbee, Osteochondral Allograft Transplantation in the Knee, Sports Med. Arthrosc. Rev., 2016, 24, 79–84.

9 T. R. Niethammer, et al., Revision surgery after third generation autologous chondrocyte implantation in the knee, Int. Orthop., 2015, 39, 1615–1622.

10 R. Shimizu, et al., Repair mechanism of osteochondral defect promoted by bioengineered chondrocyte sheet, Tissue Eng., Part A, 2015, 21, 1131–1141.

11 M. Brix, et al., Successful osteoconduction but limited cartilage tissue quality following osteochondral repair by a

cell-free multilayered nano-composite scaffold at the knee, *Int. Orthop.*, 2016, **40**, 625–632.

12 T. Welch, B. Mandelbaum and M. Tom, Autologous Chondrocyte Implantation: Past, Present, and Future, *Sports Med. Arthrosc. Rev.*, 2016, **24**, 85–91.

13 J. Malda, *et al.*, 25th anniversary article: Engineering hydrogels for biofabrication, *Adv. Mater.*, 2013, **25**, 5011–5028.

14 A. Skardal and A. Atala, Biomaterials for integration with 3-D bioprinting, *Ann. Biomed. Eng.*, 2015, **43**, 730–746.

15 T. Jungst, *et al.*, Strategies and Molecular Design Criteria for 3D Printable Hydrogels, *Chem. Rev.*, 2016, **116**, 1496–1539.

16 A. Blaeser, *et al.*, Controlling Shear Stress in 3D Bioprinting is a Key Factor to Balance Printing Resolution and Stem Cell Integrity, *Adv. Healthcare Mater.*, 2016, **5**, 326–333.

17 T. Billiet, *et al.*, A review of trends and limitations in hydrogel-rapid prototyping for tissue engineering, *Biomaterials*, 2012, **33**, 6020–6041.

18 C. B. Highley, C. B. Rodell and J. A. Burdick, Direct 3D Printing of Shear-Thinning Hydrogels into Self-Healing Hydrogels, *Adv. Mater.*, 2015, **27**, 5075–5079.

19 J. Jia, *et al.*, Engineering alginate as bioink for bioprinting, *Acta Biomater.*, 2014, **10**, 4323–4331.

20 E. Mirdamadi, N. Muselimyan, P. Koti, H. Asfour and N. Sarvazyan, Agarose Slurry as a Support Medium for Bioprinting and Culturing Freestanding Cell-Laden Hydrogel Constructs, *3D Print. Addit. Manuf.*, 2019, **6**, 158–164.

21 M. Yeo, *et al.*, An Innovative Collagen-Based Cell-Printing Method for Obtaining Human Adipose Stem Cell-Laden Structures Consisting of Core-Sheath Structures for Tissue Engineering, *Biomacromolecules*, 2016, **17**, 1365–1375.

22 K. Schacht, *et al.*, Biofabrication of cell-loaded 3D spider silk constructs, *Angew. Chem., Int. Ed. Engl.*, 2015, **54**, 2816–2820.

23 M. J. Rodriguez, *et al.*, Silk based bioinks for soft tissue reconstruction using 3-dimensional (3D) printing with in vitro and in vivo assessments, *Biomaterials*, 2017, **117**, 105–115.

24 M. C. Echave, L. Saenz del Burgo, J. L. Pedraz and G. Orive, Gelatin as Biomaterial for Tissue Engineering, *Curr. Pharm. Des.*, 2017, **23**, 3567–3584.

25 A. B. Bello, D. Kim, D. Kim, H. Park and S. H. Lee, Engineering and Functionalization of Gelatin Biomaterials: From Cell Culture to Medical Applications, *Tissue Eng., Part B*, 2020, **26**, 164–180.

26 D. F. Campos, *et al.*, Supporting Biomaterials for Articular Cartilage Repair, *Cartilage*, 2012, **3**, 205–221.

27 X. Wang, *et al.*, Gelatin-Based Hydrogels for Organ 3D Bioprinting, *Polymers*, 2017, **9**, 401.

28 Q. Hu, C. Wu and H. Zhang, Preparation and optimization of a gelatin-based biomimetic three-layered vascular scaffold, *J. Biomater. Appl.*, 2019, **34**, 431–441.

29 R. A. Bini, *et al.*, Soft nanocomposites of gelatin and poly(3-hydroxybutyrate) nanoparticles for dual drug release, *Colloids Surf., B*, 2017, **157**, 191–198.

30 M. C. Echave, *et al.*, Enzymatic crosslinked gelatin 3D scaffolds for bone tissue engineering, *Int. J. Pharm.*, 2019, **562**, 151–161.

31 T. N. Dinh, *et al.*, Gelatin Hydrogel Combined with Polydopamine Coating to Enhance Tissue Integration of Medical Implants, *ACS Biomater. Sci. Eng.*, 2018, **4**, 3471–3477.

32 K. Reiser, R. J. McCormick and R. B. Rucker, Enzymatic and nonenzymatic cross-linking of collagen and elastin, *FASEB J.*, 1992, **6**, 2439–2449.

33 M. Griffin, R. Casadio and C. M. Bergamini, Transglutaminases: nature's biological glues, *Biochem. J.*, 2002, **368**, 377–396.

34 R. Collighan, J. Cortez and M. Griffin, The biotechnological applications of transglutaminases, *Minerva Biotecnol.*, 2002, **14**, 143–148.

35 E. P. Broderick, *et al.*, Enzymatic stabilization of gelatin-based scaffolds, *J. Biomed. Mater. Res., Part B*, 2005, **72**, 37–42.

36 B. Ghiasi, Y. Sefidbakht, S. Mozaffari-Jovin, B. Gharehcheloo, M. Mehrarya, A. Khodadadi, M. Rezaei, S. O. R. Siadat and V. Uskoković, Hydroxyapatite as a biomaterial - a gift that keeps on giving, *Drug Dev. Ind. Pharm.*, 2020, **46**, 1035–1062.

37 L. Jia, Z. Duan, D. Fan, Y. Mi, J. Hui and L. Chang, Human-like collagen/nano-hydroxyapatite scaffolds for the culture of chondrocytes, *Mater. Sci. Eng., C*, 2013, **33**, 727–734.

38 X. Jiang, Y. Zhong, L. Zheng and J. Zhao, Nano-hydroxyapatite/collagen film as a favorable substrate to maintain the phenotype and promote the growth of chondrocytes cultured in vitro, *Int. J. Mol. Med.*, 2018, **41**, 2150–2158.

39 S. A. Jamal and Q. Ye, Hydroxyapatite-Based Colloidal Gels Facilitate the Proliferation and Migration of Chondrocytes and the Adhesion of Umbilical Cord Mesenchymal Stem Cells, *Int. Scholarly Res. Not.*, 2014, 935689.

40 C. Spadaccio, A. Rainer, M. Trombetta, G. Vadalá, M. Chello, E. Covino, V. Denaro, Y. Toyoda and J. A. Genovese, Poly-L-lactic acid/hydroxyapatite electrospun nanocomposites induce chondrogenic differentiation of human MSC, *Ann. Biomed. Eng.*, 2009, **37**, 1376–1389.

41 G. Calabrese, S. Forte, R. Gulino, F. Cefalì, E. Figallo, L. Salvatorelli, E. T. Maniscalchi, G. Angelico, R. Parenti, M. Gulisano, L. Memeo and R. Giuffrida, Combination of Collagen-Based Scaffold and Bioactive Factors Induces Adipose-Derived Mesenchymal Stem Cells Chondrogenic Differentiation In vitro, *Front. Physiol.*, 2017, **8**, 50.

42 Q. L. Loh and C. S. N. Choong, Three-dimensional scaffolds for tissue engineering applications : role of porosity and pore size, *Tissue Eng., Part B*, 2013, **19**, 485–502.

43 Z. Z. Zhang, D. Jiang, J. X. Ding, *et al.*, Role of scaffold mean pore size in meniscus regeneration, *Acta Biomater.*, 2016, **43**, 314–326.

44 A. Matsiko, J. P. Gleeson and F. J. O'Brien, Scaffold mean pore size influences mesenchymal stem cell chondrogenic differentiation and matrix deposition, *Tissue Eng., Part A*, 2015, **21**, 486–497.

45 A. Salamon, S. van Vlierberghe, I. van Nieuwenhove, F. Baudisch, G.-J. Graulus, V. Benecke, K. Alberti, H.-G. Neumann, J. Rychly, J. C. Martins, P. Dubruel and K. Peters, Gelatin-based hydrogels promote chondrogenic differentiation of human adipose tissue-derived mesenchymal stem cells in vitro, *Materials*, 2014, **7**, 1342–1359.

46 Y. Sun, Y. You, W. Jiang, Q. Wu, B. Wang and K. Dai, Generating ready-to-implant anisotropic menisci by 3D-bioprinting protein-releasing cell-laden hydrogel-polymer composite scaffold, *Appl. Mater. Today*, 2020, **18**, 100469.

47 Y. Sun, Y. You, W. Jiang, B. Wang, Q. Wu and K. Dai, 3D bioprinting dual-factor releasing and gradient-structured constructs ready to implant for anisotropic cartilage regeneration, *Sci. Adv.*, 2020, **6**, eeay1422.

48 Y. Sun, Y. You, W. Jiang, Z. Zhai and K. Dai, 3D-bioprinting a genetically inspired cartilage scaffold with GDF5-conjugated BMSC-laden hydrogel and polymer for cartilage repair, *Theranostics*, 2019, **9**, 6949–6961.

49 P. Sanaei-rad, T.-S. J. Kashi, E. Seyedjafari and M. Soleimani, Enhancement of stem cell differentiation to osteogenic lineage on hydroxyapatite-coated hybrid PLGA/gelatin nanofiber scaffolds, *Biologicals*, 2016, **44**, 511–516.

50 X. Yang, Y. Li, X. Liu, R. Zhang and Q. Feng, In Vitro Uptake of Hydroxyapatite Nanoparticles and Their Effect on Osteogenic Differentiation of Human Mesenchymal Stem Cells, *Stem Cells Int.*, 2018, 2036176.

51 J. Zhou, C. Xu, G. Wu, *et al.*, In vitro generation of osteochondral differentiation of human marrow mesenchymal stem cells in novel collagen-hydroxyapatite layered scaffolds, *Acta Biomater.*, 2011, **7**, 3999–4006.

52 J. Michel, M. Penna, J. Kochen and H. Cheung, Recent Advances in Hydroxyapatite Scaffolds Containing Mesenchymal Stem Cells, *Stem Cell Int.*, 2015, 305217.